Smart Agricultural Technology 3 (2023) 100100

Contents lists available at ScienceDirect

Smart Agricultural Technology

journal homepage: www.journals.elsevier.com/smart-agricultural-technology

Use of RGB images from unmanned aerial vehicle to estimate lettuce growth in root-knot nematode infested soil

Vytória Piscitelli Cavalcanti [a,*], Adão Felipe dos Santos [a], Filipe Almendagna Rodrigues [a], Willian César Terra [b], Ronilson Carlos Araújo [a], Clerio Rodrigues Ribeiro [a], Vicente Paulo Campos [b], Everlon Cid Rigobelo [c], Flávio Henrique Vasconcelos Medeiros [b], Joyce Dória [a]

[a] Department of Agriculture, Federal University of Lavras (UFLA), P.O. Box: 3037, 37.200-900, Lavras, MG, Brazil
[b] Department of Phytopathology, Federal University of Lavras (UFLA), P.O. Box: 3037, 37.200-900, Lavras, MG, Brazil
[c] Department of Plant Production, University of São Paulo State (UNESP), 14884-900 Jaboticabal, SP, Brazil

ARTICLE INFO

Keywords:
Lactuca sativa
Meloidogyne incognita
Bacillus subtilis
Biological control
Vegetation index
Vegetation cover

ABSTRACT

Lettuce (*Lactuca sativa*) is an important horticultural commodity all over the world, and its growth can be affected by root-knot nematodes (*Meloidogyne* spp.). To keep track of plant behaviors, growers are using new technologies. In this paper, aerial images were obtained using a low-cost unmanned aerial vehicle (UAV) to gather crop information in a short time giving acceptable accuracy for decision-making in the field. Evaluations were done to check the flight height interference in the image's quality for lettuce mapping, and select the best one to estimate the effect of root-knot nematode incidence on lettuce growth. In a field infested with *M. incognita*, lettuce seedlings were planted in plots treated with bionematicide and control plots. Aerial images were obtained using low-cost UAV in four flight heights performed for five weeks, along with field measurements. Images were processed and used to calculate vegetation indices (VI) and vegetation cover (VC). After lettuce harvesting, nematode eggs were extracted from plants' roots and quantified. Plots treated with bionematicide showed no difference from the control plots in eggs number and lettuce growth. Differences in VI values between the flight heights were not consistent, suggesting that VI values could be affected by the lack of luminosity calibration in each flight condition. VC values calculated from field data presented strong positive correlations with VI and VC values from UAV image data, indicating that RGB images obtained by UAV can be used in the detection of diseases that affect plant growth, as well as following up harvesting time.

1. Introduction

The development of tools to reduce the work and time spent monitoring crops in the field have ever aroused great interest of the farmers. The use of aerial images in the management of agricultural fields has been gaining more and more space in the field's routine [1–4]. The images processing provide a lot of data on the crop field in less time consuming than traditional methods [5]. By extracting information from aerial images, it is possible to delineate management zones and build cultivation guidelines according to the needs of plants in each zone. In this way, the farmers are able to check the plants growth and nutritional status, identify the best time to harvest, detect pests and diseases, being prepared to perform the precision agriculture [2,4,6–8].

Aerial images can be obtained from low-cost unmanned aerial vehicles (UAVs), increasing this technology access and, consequently, expanding its use [9]. Currently, large and small horticultural farmers use UAV images to obtain information of their crops in a short time and with acceptable accuracy to decision making in the field [10].

Lettuce (*Lactuca sativa*) is a widely consumed horticultural crop in the world and cultivated in all Brazilian regions. Plant-parasitic nematodes are soil-borne pathogens that feed mainly on the roots of susceptible plants. These phytopathogens cause billionaire losses to farmers

* Corresponding author.
E-mail addresses: vytoriapc27@gmail.com (V.P. Cavalcanti), adao.felipe@ufla.br (A.F. dos Santos), filiperodrigues@ufla.br (F.A. Rodrigues), terranema@gmail.com (W.C. Terra), ronnjkarlos7@gmail.com (R.C. Araújo), clerio.ribeiro@estudante.ufla.br (C.R. Ribeiro), vpcampos@ufla.br (V.P. Campos), everlon.cid@unesp.br (E.C. Rigobelo), flaviomedeiros@ufla.br (F.H.V. Medeiros), joyce.doria@ufla.br (J. Dória).

https://doi.org/10.1016/j.atech.2022.100100
Received 5 July 2022; Accepted 27 July 2022
Available online 28 July 2022

around the world, with root-knot nematodes responsible for most of this damage. Lettuce plants are usually susceptible to root-knot nematodes (*Meloidogyne* spp.). Depending on the nematode population level in the soil, it can cause losses of U$ 23.19 for the cultivation of 2000 lettuce plants [11]. UAV images can be used to investigate nematode-infested areas, as reported for coffee [12–14] and soybeans [15] crops, but not yet used in lettuce crop.

The aerial images quality will depend on several factor, such as the camera resolution, flight height, weather conditions, among others [16]. In horticultural crops, which are usually smaller plants, the resolution is an important factor to detect them. The smaller is the flight height, the higher will be the resolution and, consequently, the higher will be the level of detail obtained in the images [17,18]. Thus, it is necessary to identify flight heights to meet the needs of each culture. Looking to simplify the process of monitoring and detecting the occurrence of root-knot nematodes in lettuce crop as well as the reduction of the losses, in this research the objectives were to evaluate the flight height interference in the images quality for lettuce mapping, and select the best one to estimate the effect of *Meloidogyne* spp. incidence on lettuce growth and development using RGB images obtained from UAVs.

2. Material and methods

2.1. Study area

The experiment was carried out at the Center for Technology Development and Transfer – CDTT from the Federal University of Lavras – UFLA, in the municipality of Ijaci, MG, Brazil (Latitude: 21°9′48.73"S, Longitude: 44°55′2.26"W) (Fig. 1).

In a field naturally infested with *Meloidogyne incognita*, lettuce cultivar Solaris seedlings were planted in 2-meter x 1-meter plots. Twenty-four seedlings were planted per plot. The experiment consisted of some plots with the application of *Bacillus subtilis* BV09 (Biobaci®) and others without applications (control). Four repetitions (plots) were performed for each treatment (T1 = without application, and T2 = *B. subtilis* BV09 application).

2.2. Aerial images acquisition

The aerial images were obtained with a DJI Phantom 4 Advanced aircraft (Fig. 2) with the following characteristics: weight of 1388 g; diagonal size (propellers excluded) of 350 mm; maximum speed of 72 km/h; maximum angle of inclination of 42°, and maximum flight time of 30 min. The GPS/GLONASS positioning system was equipped, by default, with a 1-in. CMOS sensor to capture video (up to 4,096 × 2,160 p at 60 fps) and photos up to 20 megapixels.

The planning was performed using the free software Pix4DCapture installed on an iOS system. The flight plan was defined according to the following characteristics: speed of 3 m/s and all side with 80% overlap. The same mission was applied to four different flight heights: 10 m (GSD = 0.44 cm/pixel), 15 m (GSD = 0.66 cm/pixel), 20 m (GSD = 0.88 cm/pixel), and 25 m (GSD = 1.09 cm/pixel). The flights were performed weekly for five weeks, beginning two weeks after lettuce planting until three days before harvesting.

2.3. Image processing

The images taken from each week were processed using Agisoft PhotoScan software (Agisoft LLC, St. Petersburg, Russia). This software, based on a SfM algorithm, is superior to others in terms of precision. Also, the software provides three-dimensional points and produces a reliable data set to create dense point clouds. The input photographs can then be mosaicked and orthorectified to create the DEM by converting the point clouds into vector mesh or raster digital elevation models (DEMs) [19].

To generate the orthomosaic, the images were alignment using the photo-triangulation process and generation of a sparse point cloud, which defined the coordinate system of the terrain (Step 1). In sequence, the sparse point cloud generated in the previous step was densified providing more detailed representation of the mapped area and was also referenced the WGS 84 Zone 23S local coordinate system (Step 2). In step 3, a model was built that accurately represented the three-dimensional mapped terrain. Thus, it was possible to represent the digital surface model (DSM), and, after filtering the point cloud of the

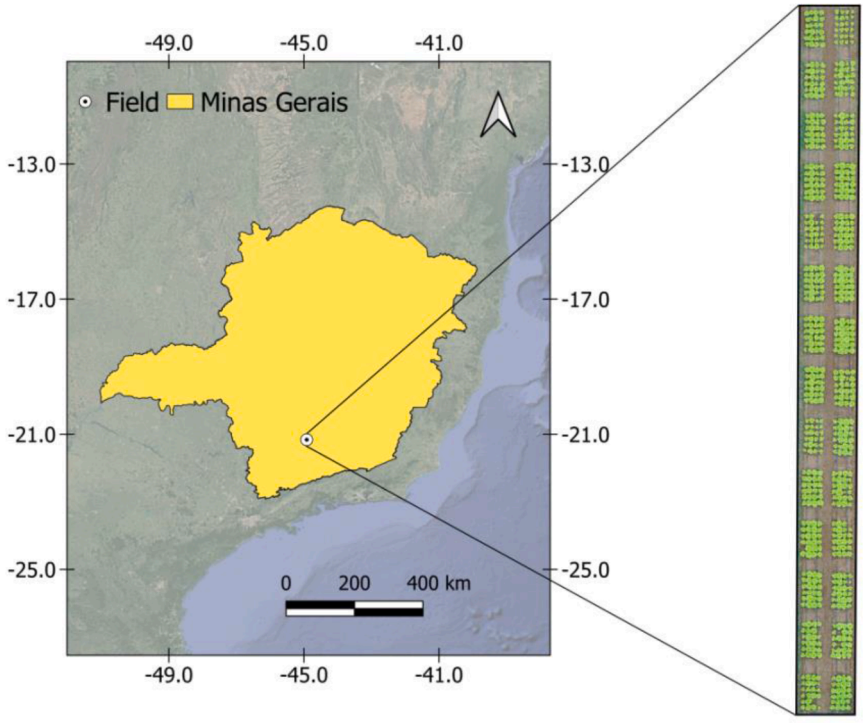

Fig. 1. Location of the experimental area.

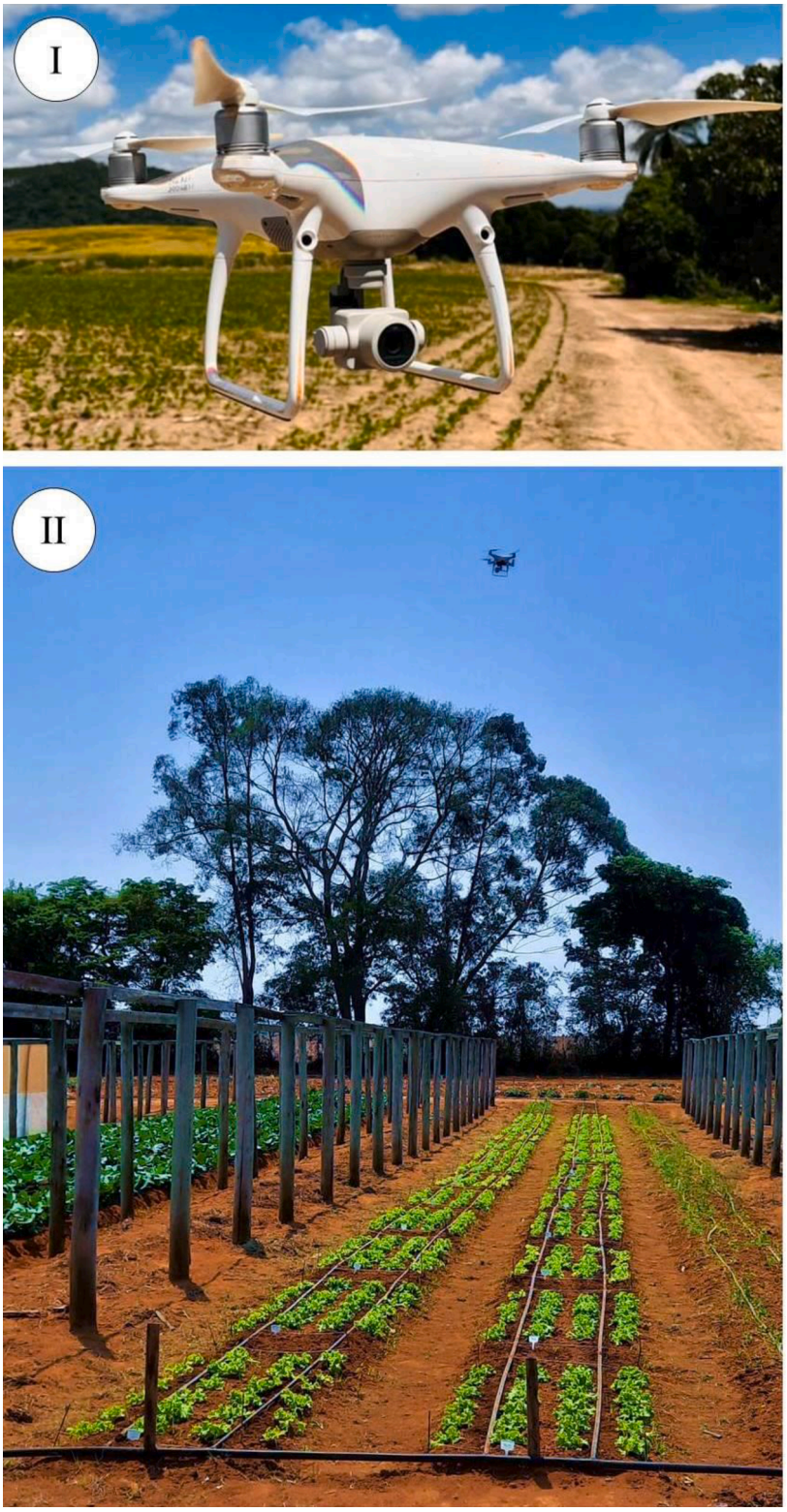

Fig. 2. DJI Phantom 4 Advanced aircraft (I) and image capturing process (II).

soil, it was possible to visualize the digital terrain model (DTM). In step 4, the texture was applied to the model obtained in the previous step to improve the visual appearance and distinction between objects. Step 5 consisted of the creation of the DEM. The generated products were two-dimensional raster format representations of the DSM and DTM. Lastly, the orthomosaic was generated in step 6.

Despite the low-cost UAVs produce georeferenced images (geotags), it is necessary to adjust the actual positioning with the aid of Ground Control Point (GCP) to improve the accuracy, especially when you are working with different flight days [20]. The Qgis software (QGIS Development Team, Open Source Geospatial Foundation) was used to identify and align the coordinates in all orthomosaic.

2.4. Vegetation cover calculation

The process used to calculate the vegetation cover was performed in QGIS starting by removing the soil, as described below and summarized in Fig. 3.

After the align images (orthomosaic image), the soil reflectance was removed from plant reflectance, in Qgis software, as follows: a shapefile was created for soil and plant classes (step 1) and a vegetation index was calculated (step 2). In step 3, soil and vegetation were segmented through the images classification with training using the supervisor classification plug-in in QGIS dzetsaka: Classification tool (https://github.com/nkarasiak/dzetsaka/). Then, the file with soil and vegetation segmented was poligonyzed, from raster to vector (step 4). In vector symbology, the options 'classify categorized' and 'enable editing' were selected to disable vegetation, select soil and delete all soil portion, remaining only vegetation portion (step 5). In geoprocessing tools, the option 'Buffer(s)' was selected to change the distance from 10 to 0.0001 meters (step 6). In step 7, the vegetation index raster file was cliped by the mask layer using the vectorized file with only vegetation portion, finally obtaining the file with only plant reflectance.

After removing the soil, zonal statistics was used to count the number of pixels of each plot, i.e., the number of pixels of the vegetable portion (step 8). Finally, using the field calculator, the vegetation cover was calculated through the following equation (step 9):

$$\text{Vegetation cover} = \frac{((\text{pixel count in plot} \times \text{pixel size}) \times 100)}{\text{plot area}} \quad (1)$$

2.5. Vegetation index calculation

Vegetation indices based on the visible portion of the electromagnetic radiation spectrum were calculated using QGIS. The green leaf index (GLI) and excess green vegetation index (ExG) can be used to separate vegetation and soil portions in the images [21]. The vegetation indices and their equation were described in Table 1.

2.6. Field measurements

The diameter of four lettuce plants per plot was measured in the field weekly for five weeks, on the same dates as the flights. Vegetation cover from the field data was obtained by calculating the mean area per plant of the measured plants and, then, multiplying by the total number of plants in the plot area.

After harvesting, the roots were washed and the *M. incognita* eggs were extracted. The number of eggs is a parameter generally used to assess the nematode population in the soil, and is directly related to the damage caused by this pathogen. To remove the eggs from the root system, the roots of each plant were cut and shaken in a blender using NaOCl at a concentration of 0.5% for 40 s. Next, the eggs were collected in a sieve of 0.025 mm opening (500 mesh), rinsed in running water and stored in plastic tubes in the refrigerator [23]. Then the eggs suspension was cleaned following the technique described by Jenkins [24]. After this process the eggs were counted in a stereoscopic microscope using a Peters' camera, and done 3 times per plot.

Table 1
Vegetation indices based on the visible portion of the electromagnetic radiation spectrum and their equation.

Vegetation index	Equation	Reference
Green Leaf Index (GLI)	$GLI = \frac{(2 \times green - red - blue)}{(2 \times green + red + blue)}$	[21]
Excess Green Vegetation Index (ExG)	$ExG = 2 \times green - red - blue$	[22]

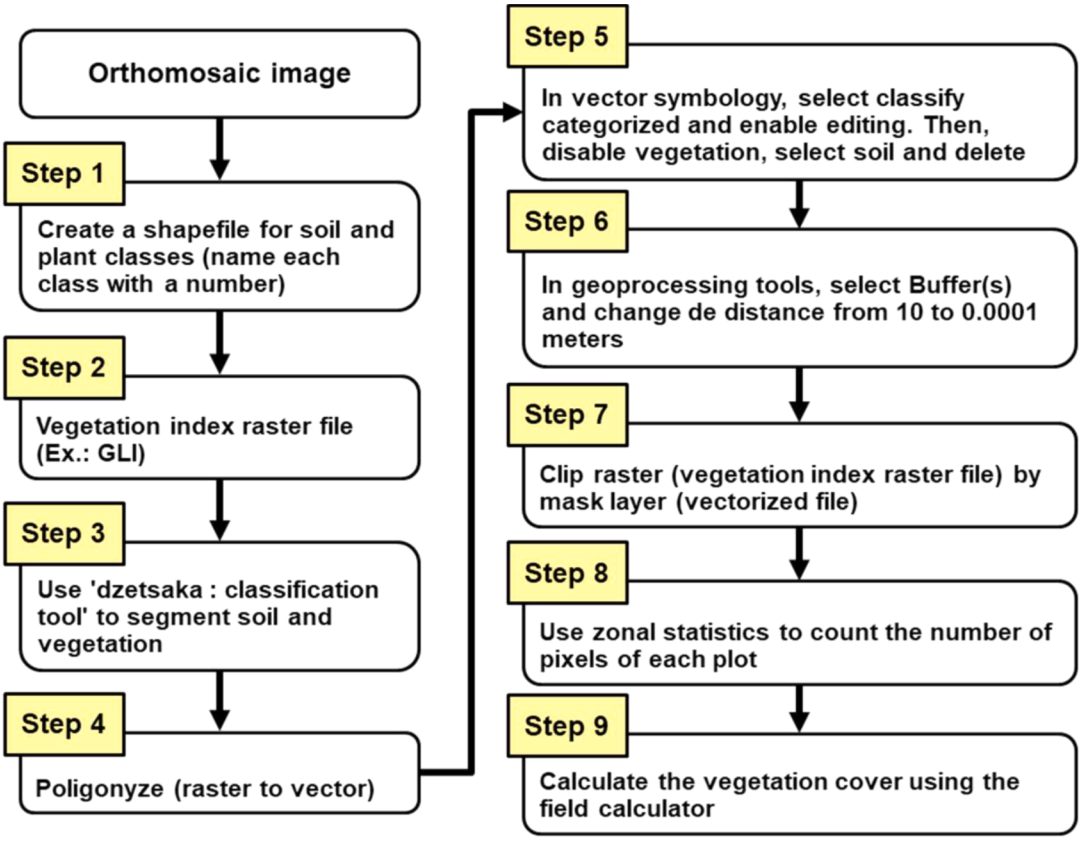

Fig. 3. The summarized processes to remove the soil for vegetation cover calculation in QGIS.

2.7. Data analysis

Shapiro–Wilk test was used to determine the normality of the data and Levene's test was performed to assess the homogeneity of variance. Then, the data were submitted to analysis of variance (ANOVA). The vegetation cover and vegetation indices means were compared by Tukey's test for each day after planting, and the eggs number and root fresh mass means were compared by Student's t test. Analysis of variance was performed to verify if there is an effect of the time on the lettuce growth, measured through the values of vegetation cover obtained from UAV image data and from field data. In addition, to assess the influence of time on lettuce growth, regression models were fitted. Pearson correlation analysis was conducted to detect the relationship between the variables, and the linear regression was conducted to describe the relationship between them. The statistical analyses were carried out by using R software [25].

3. Results

3.1. Comparing flight heights

The visible spectrum images captured in four different heights (10, 15, 20, and 25 m) show losses in image resolution as the flight height increases which reduces the details captured in the image, especially at 25 m height (Fig. 4, I). The resolution losses as the flight height increased were also observed when the vegetation indices (ExG and GLI) were calculated (Fig. 4, II and III).

Regardless of the loss of resolution as the flight height increases, significant differences were not found for the vegetation cover calculated from the aerial images obtained from 10, 15, 20, and 25 m height (Table 2). The vegetation cover calculated from the aerial images and from field data showed similar results, except at 30 DAP when the field data showed high variation, alerting to possible failures in field data collection (Table 2).

Table 2
Vegetation cover calculated from different flight heights and from field data of lettuce plants on different days after planting.

Vegetation cover Flight Heights:	15 DAP	30 DAP	44 DAP
10 m	22.569 ± 3.685 a	89.568 ± 6.055 a	95.653 ± 4.964 a
15 m	24.436 ± 3.821 a	89.581 ± 5.674 a	96.187 ± 4.448 a
20 m	25.271 ± 4.430 a	90.400 ± 5.144 a	95.922 ± 4.562 a
25 m	26.476 ± 4.085 a	91.173 ± 5.186 a	96.395 ± 4.315 a
Field data	23.066 ± 6.437 a	74.856 ± 16.862 b	90.634 ± 11.323 a

*Means followed by the same letter in the columns do not differ by Tukey test ($p<0.05$). *DAP – days after planting.*

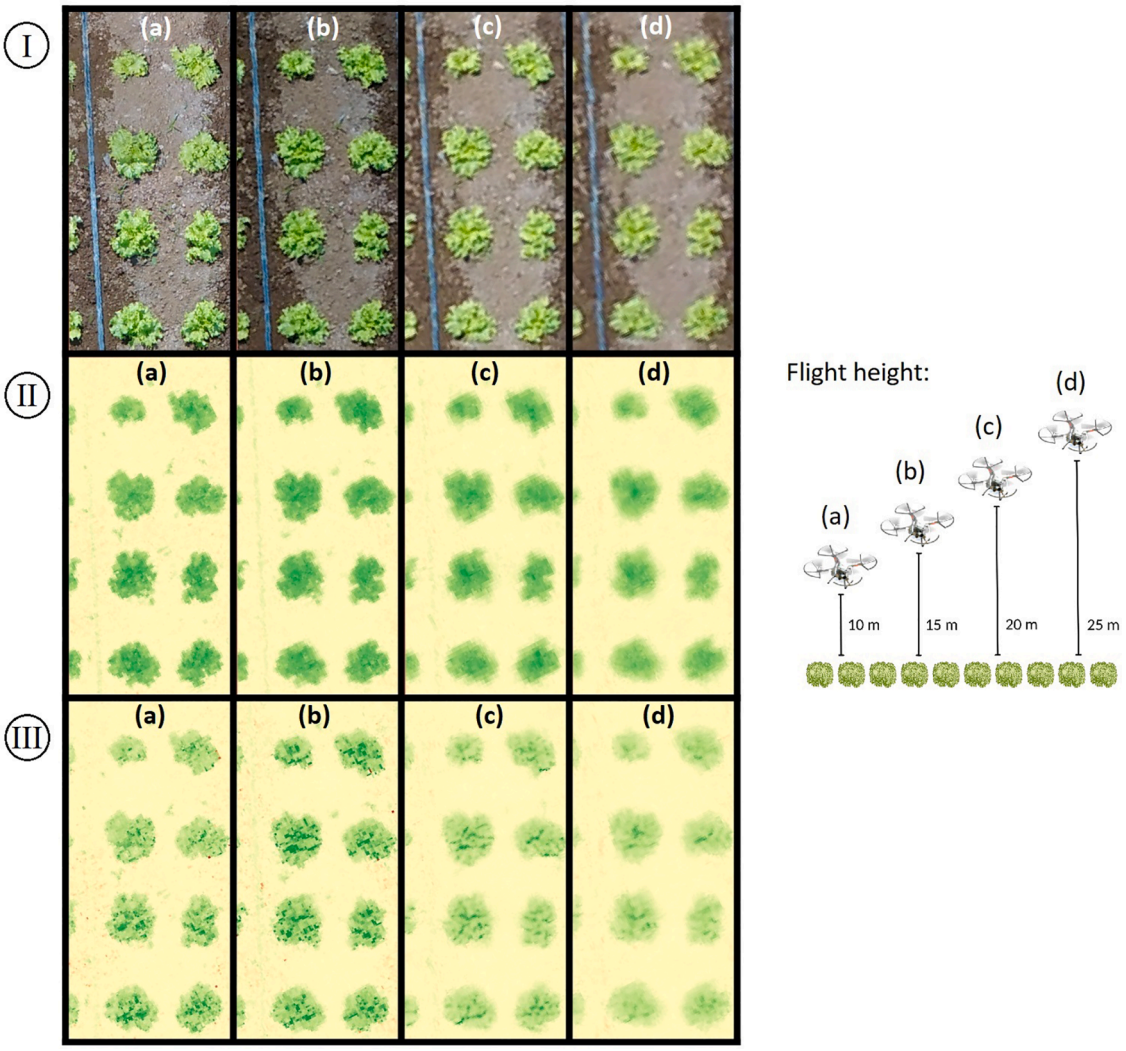

Fig. 4. Visible spectrum images (I), from lettuce plants with 15 days after planting, captured in four different heights (10 m (a), 15 m (b), 20 m (c), and 25 m (d)), and images from the vegetation indices: Excess Green Vegetation Index – ExG (II) and Green Leaf Index – GLI (III). Scale: 1:10.

The vegetation index values were compared in the different flight heights, for each evaluation day (days after planting) (Table 3). For GLI there was a significant difference ($p < 0.05$) between the flight heights in most of the days, except at 23 days after planting (DAP). At 15 DAP, the best height was 15 m, but at 23 DAP there were no differences between GLI values for all flight heights. At 30 DAP, 15, 20 and 25 m heights were better than 10 m, but at 37 DAP 10 m was the best flight height and the GLI values were decreasing when the height was increasing. In this way, the differences found in GLI values of the flight heights were not consistent over time.

For the ExG, there was no significant difference between the flight heights ($p > 0.05$) over time. Except in 37 DAP, where 10, 15 and 20 m flight heights were better than 25 m (Table 3).

3.2. Lettuce growth over time

The vegetation cover was used to evaluate the lettuce growth over time. There was no significant difference ($p > 0.05$) between the treatments without application (T1) and with the application of *Bacillus subtilis* (T2) for vegetation cover from UAV images data and from field data.

Significant differences were observed in the vegetation cover from UAV images data over time, being fitted a quadratic regression model ($p < 0.01$, $R^2 = 0.9617$, RMSE = 5.481) (Fig. 5). Using data of lettuce diameter collected manually (field data), was possible to estimate a vegetation cover by calculating the area of each plant and multiplying by the number of plants in each plots. For this vegetation cover obtained from the data collected manually in the field, it was also fitted a quadratic regression model ($p < 0.01$, $R^2 = 0.835$, RMSE = 11.758) (Fig. 5). The use of UAV images data to calculate the vegetation cover improved the accuracy in 46.61% when compared to the field measurements.

Vegetation cover values which were calculated from UAV image data and from field data presented strong and positive Pearson correlation ($r = 0.936$, $p < 0.01$). This result indicates that the aerial images obtained from UAV can be used to evaluate the lettuce growth over time, being faster and easier than going to the field and measuring plant by plant.

The GLI presented strong positive Pearson correlation with the vegetation cover values calculated from UAV image data ($r = 0.944$, $p < 0.01$), being fitted a linear regression model with reasonable precision ($R^2 = 0.891$) and accuracy (RMSE = 0.026) (Fig. 6, I). This result using UAV image data showed to be more precise than using field data, which showed positive correlation ($r = 0.856$, $p < 0.01$) and fitted a linear regression model with lower precision ($R^2 = 0.732$) (Fig. 6, I).

In contrast, when ExG was used in both types of data collection (UAV image data and field data), the Pearson correlation between vegetation cover values and the vegetation index was strong and positive with values higher than 0.9 (UAV image data: $r = 0.982$, $p < 0.01$; field data: $r = 0.936$, $p < 0.01$). In additional, the regression models had similar performance with $R^2 = 0.965$ and $R^2 = 0.877$ for UAV image and field data, respectively (Fig. 6, II).

Table 3
Vegetation indices (GLI and ExG) of lettuce plants calculated from 10, 15, 20, and 25 m flight height on different days after planting (DAP).

GLI Flight Heights:	15 DAP	23 DAP	30 DAP	37 DAP	44 DAP
10 m	0.048 ± 0.011 b	0.175 ± 0.030 a	0.240 ± 0.027 b	0.289 ± 0.022 a	0.202 ± 0.023 ab
15 m	0.061 ± 0.014 a	0.173 ± 0.028 a	0.259 ± 0.029 a	0.273 ± 0.018 b	0.211 ± 0.022 a
20 m	0.042 ± 0.013 b	0.159 ± 0.030 a	0.251 ± 0.029 ab	0.244 ± 0.022 c	0.182 ± 0.022 b
25 m	0.044 ± 0.009 b	0.166 ± 0.029 a	0.252 ± 0.031 ab	0.221 ± 0.024 d	0.184 ± 0.023 b
ExG Flight Heights:	**15 DAP**	**23 DAP**	**30 DAP**	**37 DAP**	**44 DAP**
10 m	27.339 ± 5.755 a	81.753 ± 11.046 a	136.640 ± 14.732 a	152.647 ± 11.776 a	128.837 ± 12.457 a
15 m	28.802 ± 6.044 a	81.832 ± 12.248 a	137.582 ± 14.727 a	149.790 ± 11.060 a	130.664 ± 11.158 a
20 m	25.269 ± 6.966 a	78.783 ± 12.058 a	135.442 ± 13.919 a	147.545 ± 12.583 ab	124.660 ± 11.901 a
25 m	26.070 ± 5.337 a	86.161 ± 13.218 a	133.238 ± 13.814 a	142.244 ± 13.016 b	124.689 ± 11.537 a

*Means followed by the same letter in the columns do not differ by Tukey test ($p<0.05$). *DAP – days after planting; GLI – Green Leaf Index; ExG – Excess Green Vegetation Index*.

3.3. Root-knot nematode in lettuce roots

Root-knot nematode population was evaluated by the quantification of the number of eggs in lettuce roots (Table 4). Although lettuce plants with the application of B. subtilis BV09 (T2) presented less number of eggs in their roots, significant differences ($p > 0.05$) were not found between the treatments with and without application of *B. subtilis* BV09 (Table 4). The absence of a significant difference in the number of eggs between the treatment with the application of *B. subtilis* BV09 (T2) and the control treatment (T1) may be related to the high variation in the number of eggs in lettuce roots of T1 (Table 4). It may have happened due to the lack of standardization of the initial inoculum, as the experiment was carried out in an environment with natural infestation.

There was no significant difference ($p > 0.05$) between the treatments for fresh root biomass (Table 4), and the appearance of the roots and shoots were similar among plants with and without *B. subtilis* BV09 application (Fig. 7, I and II).

4. Discussion

Using a low-cost UAV, DJI Phantom 4 Advanced aircraft, it was possible to satisfactorily calculate the vegetation cover of a lettuce plantation and differentiate lettuce plant growth between the assessment days. RGB images have been used in many research to segment plants from the overall image [26–28], providing data to calculate the vegetation cover. In this research, it was possible to calculate lettuce vegetation cover in the field through RGB images, with consistent results with the field measurements.

The vegetation indices GLI and ExG values, which presented strong positive correlation with the vegetation cover calculated from UAV and field data, can be used to identify on the maps where plants growth is affected. This technology can be applied in the evaluation of lettuce growth and in the detection of diseases that affect plant growth, such as root-knot nematode, but mainly for diseases that affect the aerial part of the plants such as the tomato spotted wilt virus on lettuce.

In horticultural crops, there are reports of flight height around 15 m for potato [18] and 20 m for lettuce [29], close to the used herein. Thus, the flight height may vary according to the level of needed detail to obtain the information for each crop. Most flight heights between 10 to 25 m are sufficient for evaluations of vegetation indices for lettuce crop.

Observing the vegetation indices values, the differences between the flight heights were not consistent, being not possible to find the best flight height for these parameters. These results lead to the conclusion that maybe the differences in the vegetation indices value between the flight heights were not caused by the flight height. Probably, these differences in vegetation indices values were caused by another factor, such as the lack of luminosity calibration in every flight. According to Woebbecke et al. [22], the excess green vegetation index (ExG) works well for both non-shaded and shaded sunlit conditions, which can explain the similarity in the ExG values for the flight heights. It corroborates the hypothesis that the inconsistent variation in the green leaf index (GLI) values can be due to the variation in the weather conditions in each flight.

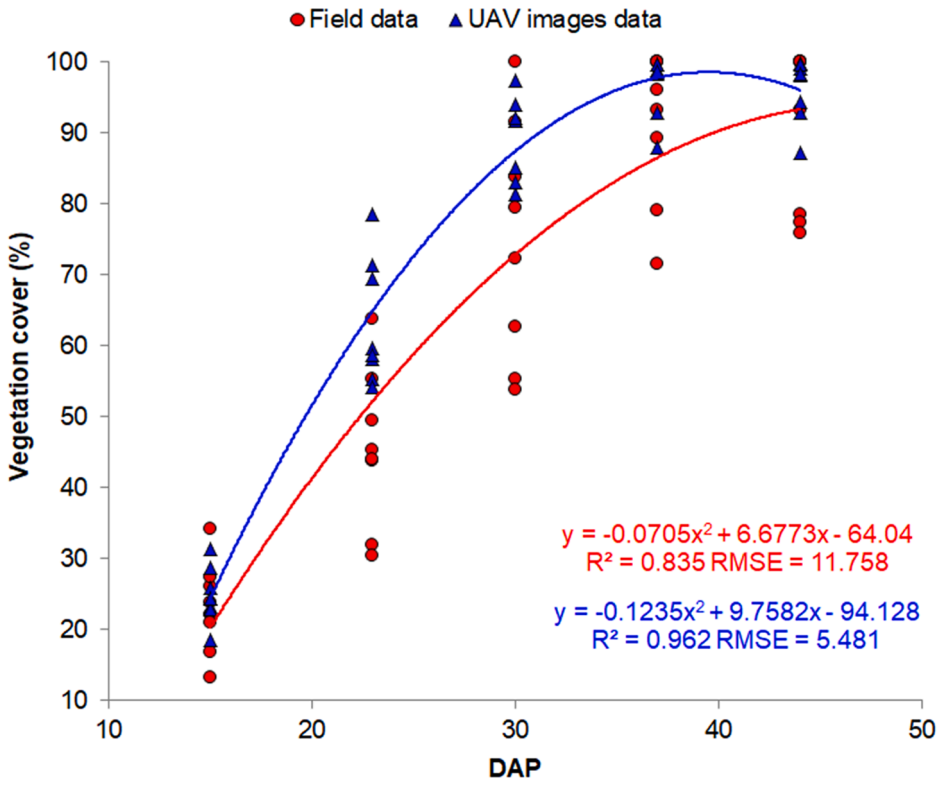

Fig. 5. Regression of lettuce growth measured by the vegetation cover (%) over time (DAP = days after planting), calculated from field data (red circle) and from UAV image data (blue triangle).

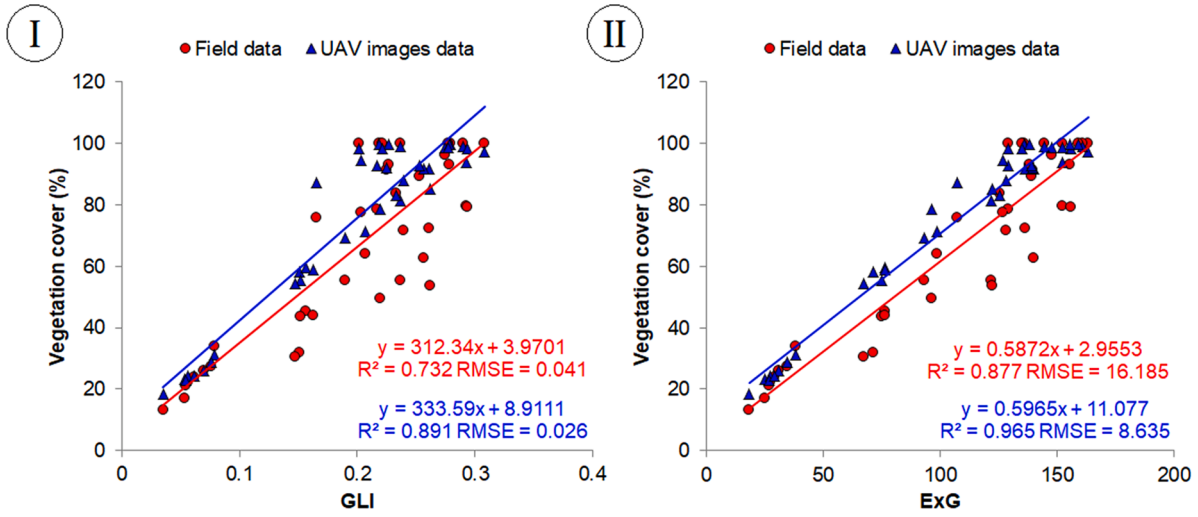

Fig. 6. Regression between the vegetation index values (I = GLI and II = ExG) and the lettuce growth measured by the vegetation cover (%) calculated from field data (red circle) and from UAV image data (blue triangle).

Table 4
Root-knot nematode population in lettuce roots with and without the application of *B. subtilis* BV09.

Treatment	N° of eggs/g of root	Fresh root biomass (g)
T1	55.671 ± 46.265 a	28.333 ± 7.835 a
T2	21.175 ± 13.247 b	32.583 ± 6.744 a

*Means followed by the same letter in the columns do not differ by Student's t-test ($p < 0.05$). *T1 – without the application of B. subtilis BV09 (control); T2 - with the application of B. subtilis BV09.*

Many researchers are using RGB images to calculate vegetation index and estimate nitrogen and chlorophyll content [6,26,30,31]. Some of the researchers who used RGB images to determine nitrogen content and chlorophyll concentration used camera support with standardized light source to capture images in greenhouse tomato [30] and lettuce [32] crops. In the field, however, it is not possible to perform the luminosity standardization in this way to capture RGB images for comparing different flights. Thus, images capture in the field requires calibration of the luminosity through the use of a panel, even before and after a flight, and a multispectral camera with an incidence light sensor [33]. Multispectral cameras have been used to calculate vegetation index and assess

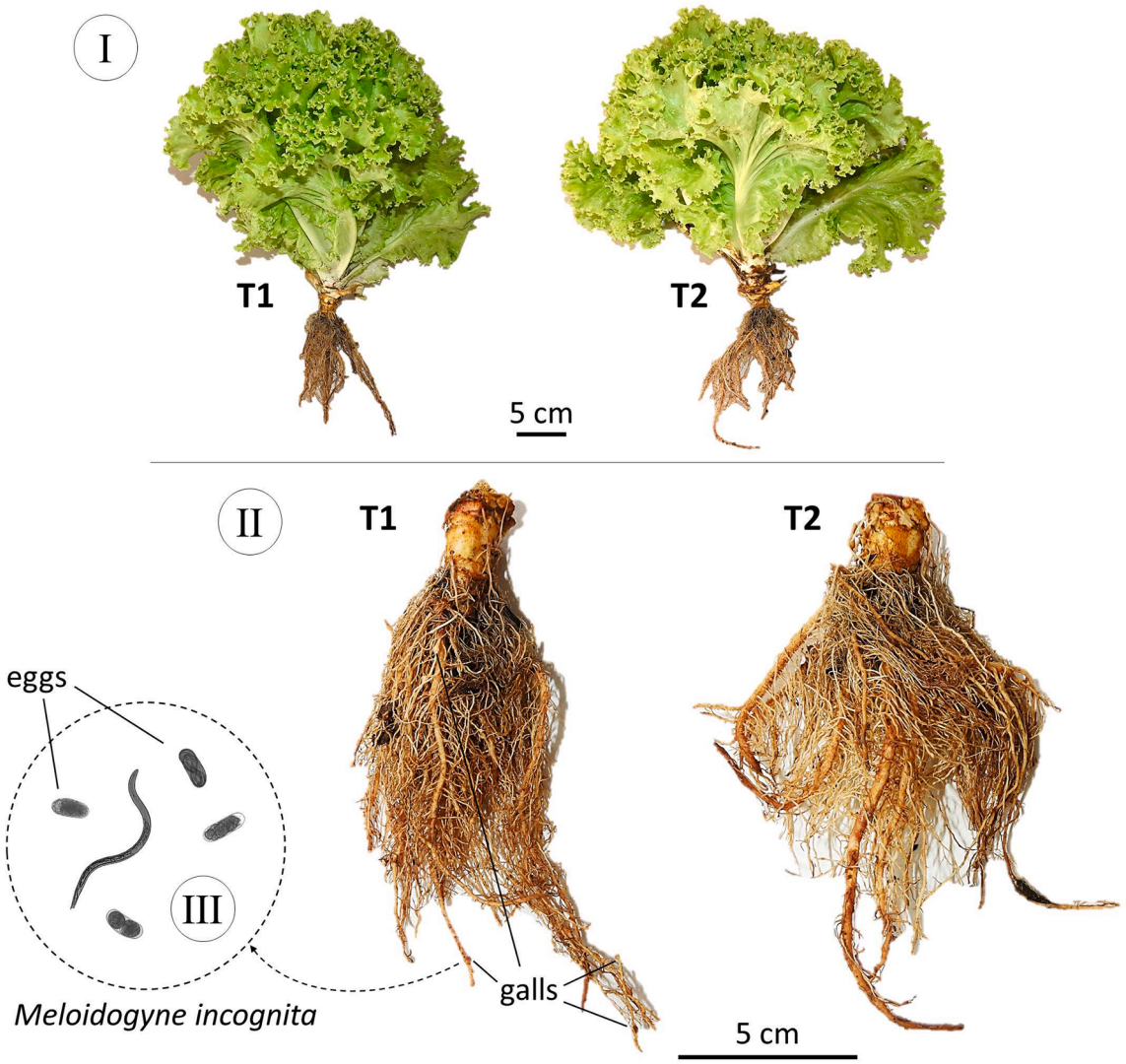

Fig. 7. Representative image of lettuce plants (I) and their roots (II) from the field which was infested with *Meloidogyne incognita*, showing the galls and eggs (III). T1 – without the application of *B. subtilis* BV09 (control); T2 – with the application of *B. subtilis* BV09.

the health of lettuce plants [9,34], as well as hyperspectral cameras have been used to assess lettuce water uptake by measuring leaf water content [35].

In this context, RGB digital cameras have the advantage of being cheaper and presenting a high resolution. However, the use of RGB images has limitations because of the high field luminosity effect and the impossibility of calibrating it, impeding the comparison of field RGB images. The color indices from RGB images can be used mainly to segment plants from the overall image and, as evaluated in this research, the vegetation indices GLI and ExG can be used to detect failures in plant growth and to identify the occurrence of diseases that affect the lettuce plant growth.

Lettuce cultivar Solaris proved to be susceptible to *M. incognita*, as found by Sgorlon et al. [36], presenting *M. incognita* infection with gall formation and eggs production (Fig. 7 and Table 4). On the other hand, this cultivar showed some tolerance to *M. incognita*, being not observed damage to lettuce plant growth.

5. Conclusions

Vegetation indices and vegetation cover calculation using RGB images captured by a low-cost UAV proved to be efficient in measuring lettuce growth over time with higher accuracy than field measurements. This technology can be applied for the detection of diseases that affect lettuce growth, as well as help following up harvesting time. RGB images should not be used to compare vegetation index values between different flights, since the light incidence and cloudiness can affect the vegetation index performance. In this case, multispectral or hyperspectral images are more suitable. Future research can assess the use of proximal sensors for plant-parasitic nematode detection in lettuce crop.

Declaration of Competing Interest

The authors declare that they have no known competing financial interests or personal relationships that could have appeared to influence the work reported in this paper.

Acknowledgment

The authors extend thanks to CAPES for granting doctorate's scholarships, to the Federal University of Lavras (UFLA) and Technology Development and Transfer Center (CDTT) for the structure provided to carry out the experiments and for the support of the technicians and professors. Thanks to the institutions: FAPEMIG, CNPq, and CAPES for providing the necessary equipment and technical support for the experiments. Thanks to Grupo Vittia for providing the Biobaci® and

technical support. Thanks to Hugo Nunes Martins Nogueira for assisting in obtaining the UAV images and to Sansão Augusto Germano, Natalia Bernardes Machado, Otávio Bernardes Machado, Regiane Alves Belizario, Kamilly Maria Fernandes Fonseca, Brenda Miriam Silva and Maria Luiza Paiva de Oliveira for assisting in field measurements.

References

[1] V. Choudhary, L. Prasad, Morpho-pathological, genetic variations and population structure of *Sclerotinia sclerotiorum*, Int. J. Plant Res. 25 (2012) 178–183.
[2] E. Raparelli, S. Bajocco, A bibliometric analysis on the use of unmanned aerial vehicles in agricultural and forestry studies, Int. J. Remote Sens. 40 (2019) 9070–9083, https://doi.org/10.1080/01431161.2019.1569793.
[3] U.R. Mogili, B.B.V.L. Deepak, Review on application of drone systems in precision agriculture, Proc. Comput. Sci. 133 (2018) 502–509, https://doi.org/10.1016/j.procs.2018.07.063.
[4] J. Barbedo, A review on the use of unmanned aerial vehicles and imaging sensors for monitoring and assessing plant stresses, Drones 3 (2019) 40, https://doi.org/10.3390/drones3020040.
[5] A. Vibhute, S.K. Bodhe, Applications of image processing in agriculture: a survey, Int. J. Comput. Appl. 52 (2012) 34–40, https://doi.org/10.5120/8176-1495.
[6] Y. Fu, G. Yang, Z. Li, X. Song, Z. Li, X. Xu, P. Wang, C. Zhao, Winter wheat nitrogen status estimation using UAV-based RGB imagery and gaussian processes regression, Remote Sens. 12 (2020) 3778, https://doi.org/10.3390/rs12223778.
[7] L. Yubin, D. Xiaoling, Z. Guoliang, Advances in diagnosis of crop diseases, pests and weeds by UAV remote sensing, Smart Agric. 1 (2019) 1–19.
[8] G. Grenzdörffer, A. Engel, B. Teichert, The photogrammetric potential of low-cost UAVs in forestry and agriculture, Int. Arch. Photogramm. Remote Sens. Spat. Inf. Sci. 31 (2008) 1207–1214.
[9] G. Cucho-Padin, H. Loayza, S. Palacios, M. Balcazar, M. Carbajal, R. Quiroz, Development of low-cost remote sensing tools and methods for supporting smallholder agriculture, Appl. Geomat. 12 (2020) 247–263, https://doi.org/10.1007/s12518-019-00292-5.
[10] B.K. Handique, C. Goswami, C. Gupta, S. Pandit, S. Gogoi, R. Jadi, P. Jena, G. Borah, P.L.N. Raju, Hierarchical classification for assessment of horticultural crops in mixed cropping pattern using uav-borne multi-spectral sensor, Int. Arch. Photogramm. Remote Sens. Spat. Inf. Sci. XLIII-B3-2 (2020) 67–74, https://doi.org/10.5194/isprs-archives-XLIII-B3-2020-67-2020.
[11] L.K.C. Rabello, A. Oliveira Gongalves, T.P. da Cruz, F. Domingo Zinger, W.C. de Jesus Júnior, L. Lagen Rodrigues, A.F. de Souza, W. Bucker Moraes, F. Ramos Alves, Quantification of damage and yield losses caused by Root-knot nematode in lettuce in Brazil, Idesia (Arica) 39 (2021) 121–130, https://doi.org/10.4067/s0718-34292021000200121.
[12] C.A.M. De Abreu Júnior, G.P. Vinhal, L.C. Moura Xavier, G.D. Martins, B.S. Vieira, Mapeamento de nematoides na cultura cafeeira a partir de imagens multiespectrais obtidas por aeronaves remotamente pilotadas, Caminhos Geogr. 21 (2020), https://doi.org/10.14393/RCG217651255.
[13] A.J. Oliveira, G.A. Assis, E.R. Faria, J.R. Souza, K.C.T. Vivaldini, V. Guizilini, F. Ramos, C.T.C. Mendes, D.F. Wolf, Analysis of nematodes in coffee crops at different altitudes using aerial images, in: 2019 27th European Signal Processing Conference, IEEE, 2019, pp. 1–5, https://doi.org/10.23919/EUSIPCO.2019.8902734.
[14] A.J. Oliveira, G.A. Assis, V. Guizilini, E.R. Faria, J.R. Souza, Segmenting and detecting nematode in coffee crops using aerial images (Eds.), in: D. Tzovaras, D. Giakoumis, M. Vincze, A. Argyros (Eds.), Computer Vision Systems ICVS 2019. Lecture Notes in Computer Science, Springer, Cham., 2019, pp. 274–283, https://doi.org/10.1007/978-3-030-34995-0_25.
[15] B.H.T. Arantes, V.H. Moraes, A.M. Geraldine, T.M. Alves, A.M. Albert, G.J. da Silva, G. Castoldi, Spectral detection of nematodes in soybean at flowering growth stage using unmanned aerial vehicles, Ciência Rural 51 (2021), https://doi.org/10.1590/0103-8478cr20200283.
[16] T. Berteška, B. Ruzgienė, Photogrammetric mapping based on UAV imagery, Geod. Cartogr. 39 (2013) 158–163, https://doi.org/10.3846/20296991.2013.859781.
[17] J. Peña, J. Torres-Sánchez, A. Serrano-Pérez, A. de Castro, F. López-Granados, Quantifying efficacy and limits of unmanned aerial vehicle (UAV) technology for weed seedling detection as affected by sensor resolution, Sensors 15 (2015) 5609–5626, https://doi.org/10.3390/s150305609.
[18] S. Sankaran, L.R. Khot, C.Z. Espinoza, S. Jarolmasjed, V.R. Sathuvalli, G. J. Vandemark, P.N. Miklas, A.H. Carter, M.O. Pumphrey, N.R. Knowles, M. J. Pavek, Low-altitude, high-resolution aerial imaging systems for row and field crop phenotyping: a review, Eur. J. Agron. 70 (2015) 112–123, https://doi.org/10.1016/j.eja.2015.07.004.
[19] J.T. Dietrich, Riverscape mapping with helicopter-based structure-from-motion photogrammetry, Geomorphology 252 (2016) 144–157, https://doi.org/10.1016/j.geomorph.2015.05.008.
[20] D. Gómez-Candón, A.I. De Castro, F. López-Granados, Assessing the accuracy of mosaics from unmanned aerial vehicle (UAV) imagery for precision agriculture purposes in wheat, Precis. Agric. 15 (2014) 44–56, https://doi.org/10.1007/s11119-013-9335-4.
[21] F.Z. Bassine, A. Errami, M. Khaldoun, Vegetation recognition based on UAV image color index, in: 2019 IEEE International Conference on Environment and Electrical Engineering 2019 IEEE Ind, Commercial Power Systems Europe (EEEIC /I&CPS Eur., IEEE, 2019, pp. 1–4, https://doi.org/10.1109/EEEIC.2019.8783830.
[22] D.M. Woebbecke, G.E. Meyer, K. Von Bargen, D.A. Mortensen, Color indices for weed identification under various soil, residue, and lighting conditions, Trans. ASAE 38 (1995) 259–269, https://doi.org/10.13031/2013.27838.
[23] R.S. Hussey, K.R. Barker, A comparison of methods for colecting inocula of meloidogyne spp including a new technique, Plant Dis. Rep. 57 (1973) 1025–1028.
[24] W.R. Jenkins, A rapid centrifugal-flotation technique for separating nematodes from soil, Plant Dis. Rep. 48 (1964) 692.
[25] R Core Team, R: A language and environment for statistical computing, (2019). https://www.r-project.org/.
[26] J. Torres-Sánchez, J.M. Peña, A.I. de Castro, F. López-Granados, Multi-temporal mapping of the vegetation fraction in early-season wheat fields using images from UAV, Comput. Electron. Agric. 103 (2014) 104–113, https://doi.org/10.1016/j.compag.2014.02.009.
[27] J. Kim, S. Kang, B. Seo, A. Narantsetseg, Y. Han, Estimating fractional green vegetation cover of Mongolian grasslands using digital camera images and MODIS satellite vegetation indices, GIScience Remote Sens. 57 (2020) 49–59, https://doi.org/10.1080/15481603.2019.1662166.
[28] D.G. Fernández-Pacheco, D. Escarabajal-Henarejos, A. Ruiz-Canales, J. Conesa, J. M. Molina-Martínez, A digital image-processing-based method for determining the crop coefficient of lettuce crops in the southeast of Spain, Biosyst. Eng. 117 (2014) 23–34, https://doi.org/10.1016/j.biosystemseng.2013.07.014.
[29] G.M. Maciel, R.B. de A. Gallis, R.L. Barbosa, L.M. Pereira, A.C.S. Siquieroli, J. Vitória Miranda Peixoto, Image phenotyping of inbred red lettuce lines with genetic diversity regarding carotenoid levels, Int. J. Appl. Earth Obs. Geoinf. 81 (2019) 154–160, https://doi.org/10.1016/j.jag.2019.05.016.
[30] A. Mercado-Luna, E. Rico-García, A. Lara-Herrera, G. Soto-Zarazúa, R. Ocampo-Velázquez, R. Guevara-González, G. Herrera-Ruiz, I. Torres-Pacheco, Nitrogen determination on tomato (Lycopersicon esculentum Mill.) seedlings by colour image analysis (RGB), Afr. J. Biotechnol. 9 (2010) 5326–5332. https://www.ajol.info/index.php/ajb/article/view/92074/81517.
[31] M.M. Saberioon, M.S.M. Amin, A.R. Anuar, A. Gholizadeh, A. Wayayok, S. Khairunniza-Bejo, Assessment of rice leaf chlorophyll content using visible bands at different growth stages at both the leaf and canopy scale, Int. J. Appl. Earth Obs. Geoinf. 32 (2014) 35–45, https://doi.org/10.1016/j.jag.2014.03.018.
[32] M.S. Odabas, H. Simsek, C.W. Lee, İ. İseri, Multilayer perceptron neural network approach to estimate chlorophyll concentration index of lettuce (Lactuca sativa L, Commun. Soil Sci. Plant Anal. 48 (2017) 162–169, https://doi.org/10.1080/00103624.2016.1253726.
[33] E.R. Hunt, C.S.T. Daughtry, What good are unmanned aircraft systems for agricultural remote sensing and precision agriculture? Int. J. Remote Sens. 39 (2018) 5345–5376, https://doi.org/10.1080/01431161.2017.1410300.
[34] D.D.W. Ren, S. Tripathi, L.K.B. Li, Low-cost multispectral imaging for remote sensing of lettuce health, J. Appl. Remote Sens. 11 (2017), 016006, https://doi.org/10.1117/1.JRS.11.016006.
[35] R.J. Murphy, B. Whelan, A. Chlingaryan, S. Sukkarieh, Quantifying leaf-scale variations in water absorption in lettuce from hyperspectral imagery: a laboratory study with implications for measuring leaf water content in the context of precision agriculture, Precis. Agric. 20 (2019) 767–787, https://doi.org/10.1007/s11119-018-9610-5.
[36] L.F.F. Sgorlon, E.H.C. Silva, R.S. Soares, H.O. Borges, G.M.M. Diniz, L.T. Braz, P.L. M. Soares, Host status of crispy-leaf lettuce cultivars to root-knot nematodes, Biosci. J. 34 (2018) 1319–1325, https://doi.org/10.14393/BJ-v34n5a2018-39387.